An evaluation of different coordinate frames in order to detect polarized virtual photons in relativistic heavy ion collisions

Quark Physics Laboratory Department of Physics
Hiroshima University

M146985
Yosuke Ueda

February 10th, 2016

Supervisor : Associate Prof. Kenta Shigaki
Primary Examiner : Associate Prof. Kenta Shigaki
Examiner : Prof. Yasushi Fukazawa

Abstract

In relativistic heavy ion collisions, a strong magnetic field is generated. When the nuclei having large charges which are accelerated to nearly the light speed collide off-centered in a small space of ˜10 fm, the intense magnetic field is created. The strength of magnetic field amounts to ˜10^{19} Gauss. It is the strongest in our universe. In the magnetic field, interesting effects, such as chiral magnetic effects, synchrotron radiation of quark, and photon decay, may occur. Detections of the intense magnetic field, however, has not been realized. In this thesis, we discuss the feasibility and methods of its detection.

In an intense magnetic field, the electron and positron from a virtual photon decay are asymmetric due to effects of electron loops of virtual photon in a magnetic field, and this electron-positron polarization depends on the direction of the magnetic field. We can hence detect the magnetic field by detection of virtual photon polarization. We use polarization frames used in J/Ψ polarization measurement to detect the virtual photon polarization.

First, I evaluate the detection feasibility of virtual photon polarization in the PHENIX experiment based on the statistics. We use the AuAu collision data at $\sqrt{s_{NN}} = 200GeV$ in 2004 for this evaluation. As a result, the feasibility to detect virtual photon polarization is ˜0.2σ. Also the estimated feasibility using the data in 2010 is ˜0.6σ, and it using the data in 2014 is more order.

Next, I estimate the detection feasibility of virtual photon polarization using three different polarization frames, detection Helicity (HX) frame, Gottfried-Jackson (GS) frame, and Collins-Soper (CS) frame. I tested three polarization cases, no-polarization, perpendicular, and parallel with respect to the direction of magnetic field. I compare these and decide that CS frame is the most useful frame for detection of polarization. Also I simulate the polarization measurement with the polarization rate to estimate the feasibility.

Contents

1 Introduction **6**
- 1.1 Relativistic Heavy Ion collisions . . . 6
  - 1.1.1 Space-Time development of QGP . . . 6
- 1.2 Generation of a intense magnetic field . . . 7
  - 1.2.1 Physics phenomenon in a intense magnetic field . . . 9
- 1.3 Virtual photon polarization by a intense magnetic field . . . 10
- 1.4 Virtual photon in to measure the polarization . . . 11
- 1.5 Theoretical feasibility of magnetic field detection . . . 11
- 1.6 Purpose . . . 13

2 Experiment **14**
- 2.1 RHIC accelerator . . . 14
  - 2.1.1 PHENIX experiment . . . 14
  - 2.1.2 PHENIX detectors . . . 16
- 2.2 LHC accelerator . . . 17
  - 2.2.1 ALICE experience . . . 18
  - 2.2.2 ALICE detectors . . . 19

3 Method **22**
- 3.1 Definition of polarization frames . . . 22
  - 3.1.1 Feature of each polarization frame . . . 22
  - 3.1.2 Definition of angle on polarization frame . . . 25
- 3.2 Calculation of polarization parameter . . . 25

4 Simulation **28**
- 4.1 Method of simulation . . . 28
- 4.2 Hijing event . . . 28
  - 4.2.1 Same Hijing simulation . . . 28
  - 4.2.2 Mixed Hijing simulation . . . 29
- 4.3 Signal event . . . 31
- 4.4 Signal-Hijing event . . . 31
- 4.5 Subtraction of background effect . . . 32

5 Result **33**
- 5.1 Selection of good frame . . . 33
- 5.2 Polarization measurement with detectors . . . 34
  - 5.2.1 ALICE detector . . . 34
  - 5.2.2 PHENIX detector . . . 35
- 5.3 With polarization rate . . . 36

6 Conclusion **38**

7 Acknowledgement **39**

List of Figures

1 Schematic of heavy ion collision [1] . . . 6
2 Accelerated nuclei collision [2] . . . 7
3 Space-time evolution of a heavy ion collision [3] . . . 8
4 Generation of magnetic field [5] . . . 9
5 Diagram of virtual photon loop . . . 10
6 Invariant mass distribution of electron-positron pair for AuAu collision (M.B., $1.0 < p_T < 1.5\ GeV/c$) [7] . . . 12
7 Fraction of the direct photon component as a function of p_T [7] . . . 12
8 RHIC accelerator [11] . . . 14
9 PHENIX detector [12] . . . 15
10 EMC detector . . . 16
11 RICH detector [14] . . . 17
12 DCH detector [15] . . . 17
13 LHC accelerator [1] . . . 18
14 ALICE detector [1] . . . 19
15 ITS detector [16] . . . 20
16 TPC detector [16] . . . 20
17 TOF detector [16] . . . 21
18 Polarization frames . . . 22
19 Definition of HX frame on lepton pair rest frame . . . 23
20 Definition of GJ frame on lepton pair rest frame . . . 24
21 Definition of CS frame on lepton pair rest frame . . . 24
22 Definition of zenith angle and azimuth angle . . . 25
23 Aanisotropy of zenith angle [18] . . . 26
24 Anisotropy of azimuth angle [18] . . . 27
25 Deviation from good frame [18] . . . 27
26 Polarized lepton pair as polarization case . . . 28
27 $cos\theta$ distribution by Same Hijing event . . . 29
28 Image of p_T selection in cut region [7] . . . 29
29 $cos\theta$ distribution as each polarization frames . . . 30
30 λ_θ of Hijing event . . . 30
31 $cos\theta$ distribution of signal as each polarization case . . . 31
32 $cos\theta$ distribution on each polarization case . . . 31
33 Subtracted $cos\theta$ distribution on each polarization case . . . 32
34 Corrected $cos\theta$ distribution on each polarization case . . . 32
35 $\lambda_\theta, \lambda_\phi$ and $\lambda_{\theta\phi}$ at all acceptance . . . 33
36 λ_θ at ALICE acceptance . . . 35
37 λ_θ at PHENIX . . . 36
38 λ_θ at all, ALICE and PHENIX acceptance . . . 37

List of Tables

1 Magnet field strength [4] 8
2 List of used value to estimate the theoretical feasibility 13
3 List of $\lambda_\theta, \lambda_\phi$ and $\lambda_{\theta\phi}$ at all acceptance 33
4 List of λ_θ at ALICE 34
5 List of λ_θ at PHENIX acceptance 35
6 List of λ_θ at with acceptance cut 36

1 Introduction

1.1 Relativistic Heavy Ion collisions

Quarks and gluons are confined in a hadron such as a proton or a neutron by strong interaction in the present universe. In the early universe at a high temperature within hundreds of thousandth second from the big bang, however, quarks and gluons are deconfined. Deconfined quarks and gluons are called the"Quark Gluon Plasma (QGP)". To know the property of the elementary particles, the research of QGP is extremely important. The way to do this is relativistic heavy ion collisions at Relativistic Heavy Ion Collider (RHIC) at Brookhaven National Laboratory (BNL) and at Large Hadron Collider (LHC) at European Organization for Nuclear Research (CERN).

1.1.1 Space-Time development of QGP

The space-time development is the below.

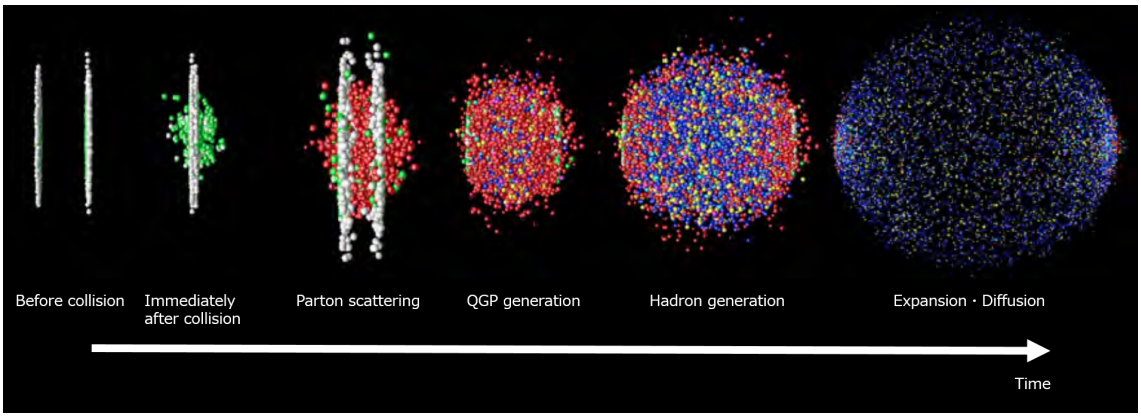

Figure 1: Schematic of heavy ion collision [1]

1. The nuclei are accelerated to near the light velocity. At this time, nuclei look like disk-shaped with Lorentz contraction.

2. The accelerated nuclei collide. The nuclei do not always collide at the center, collisions is often slipped (these are called the non-central collision). In the case of non-central collisions, the overlap region of the nuclei is interacted. This interacted part is called participants, and the non-interacted and pass part is called the spectator (Figure 2).

   The degree of central collision is called impact parameter. It is defined as the distance between the centers of the nuclei when the colliding nuclei are passing, namely the distance of closest approach of nuclei. Also, the plane consisting of the impact parameter and the beam axis, is called the reaction plane.

3. The temperature and energy density of the participants are increasing. When the temperature of the participants is over the phase transition temperature, the quarks

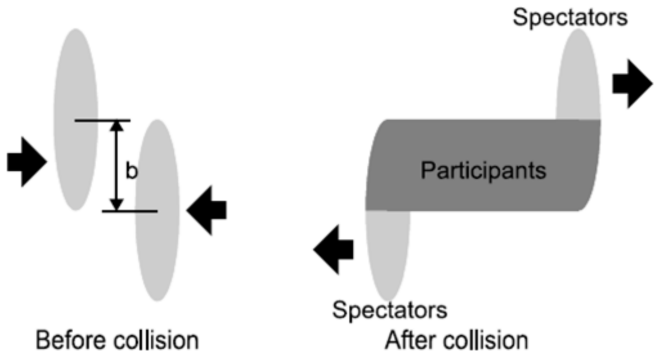

Figure 2: Accelerated nuclei collision [2]

and gluons (these are called "parton") are deconfined. The partons are scattered without bound and collide one another, and new partons are generated. QGP is this state.

4. QGP expands at near the light velocity with the high pressure inside. This rapid expansion decreases the temperature and density, and re-connecting partons form hadrons. The scattering and interaction, however, occur between the partons, and the hadrons transfer their energy with inelastic scattering. Low energy particles receiving energy with this inelastic scattering excite to higher energy levels. The high energy particles transit the original energy with radiation of light particles or decay, and new particles are continually generated.

5. The inelastic scattering of hadrons and the interaction between partons decrease the temperature and density. When new hadrons are no longer generated, the specie and amount of hadrons are fixed. It is called "chemical freezeout". The hadrons still collide one another with elastic collisions.

6. Distance between particles get over the mean free path with the consecutive expansion. The elastic collisions no longer occur, and the momenta of the particles are fixed. It is called "kinematic freezeout".

7. The generated particles are spread in a stable status. These particles are detected using detectors.

1.2 Generation of a intense magnetic field

The intense magnetic field is generated with relativistic heavy ion collision. The maximum strength of it is 10^{19} Gauss. This strength far better than artificial stable magnetic fields (4.5×10^5 Gauss), and it get even over the magnetic field of magnetor which is a neutron star and get attention to have a strong magnetic field (10^{15} Gauss). Therefore the magnetic field with heavy ion collision is considered that it is the strongest magnetic field in the universe (Table 1).

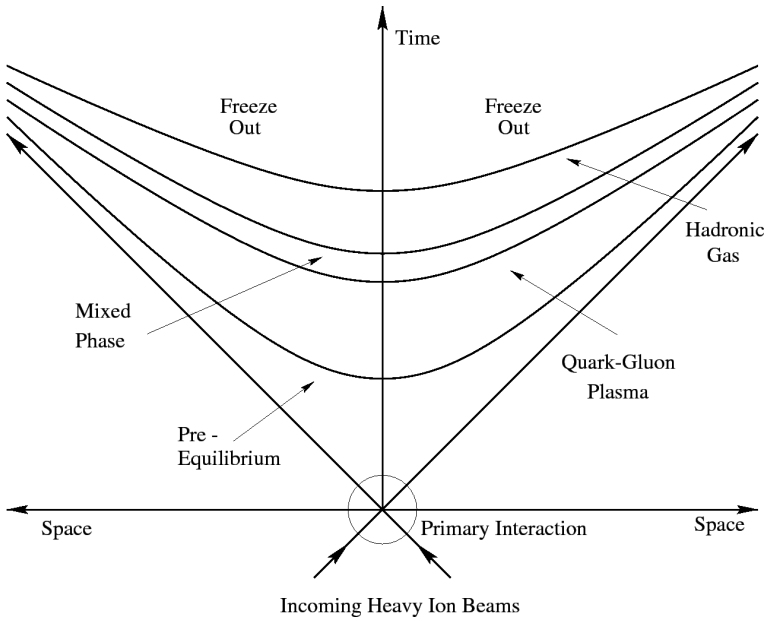

Figure 3: Space-time evolution of a heavy ion collision [3]

System	Strength [Gauss]
The Earth magnetic field on N magnet pole	0.6
A common magnet	100
The magnetic field in strong sunspots	4000
The most strong and sustained magnetic field in laboratory	4.5×10^5
The most strong and only briefly magnetic field in laboratory	10^7
Magnetor	10^{14-15}
The generated magnetic field with relativistic heavy ion collision on RHIC	10^{18}
The generated magnetic field with relativistic heavy ion collision on LHC	10^{19}

Table 1: Magnet field strength [4]

The equation (1) shows that the charged particles with velocity $\boldsymbol{v}$ creates the magnetic field at time t, position $\boldsymbol{r}, \boldsymbol{r'}$. quote the Lienard-Wiechert Potential,

$$B(\mathbf{r}, t) = \frac{e\mu_0}{4\pi} \frac{\boldsymbol{v} \times \boldsymbol{R}}{\boldsymbol{R}^3} \frac{1 - v^2/c^2}{[1 - (v/c)^2 sin\phi_{Rv}]^{3/2}}. \tag{1}$$

In this equation, $\boldsymbol{R} = \boldsymbol{r} - \boldsymbol{r'}$, μ_0 is the magnetic permeability in the vacuum, ϕ_{Rv} is the angle between $\boldsymbol{R}$ and $\boldsymbol{v}$. Z is the amount of charge, e is the elementary charge and c is the light velocity. This equation is applied to the magnetic field generation with heavy ion collision. Also, the life time of generated magnetic field is difference between the spectator part and participant part. In the case that the beam axis is z axis, and the vertical axis to z axis and a reaction plane is y axis, spectators have the z axis momentum and shift the x axis direction with passing another. At that time, the magnetic field is generated to the vertical direction to the reaction plane. In short, the direction of magnetic field is always on xy plane. It is more strong than a magnetic field of participant, but spectators runs away at near the light velocity because spectators do not collision. Therefore this

magnetic field is rapidly decreased.

On the other hand, the participant do not run away like spectators. Collisional particles is rolling around the vertical direction to the reaction plane with angular momentum. The life time of it is more longer than the magnetic field of spectator. The angular momentum is resisted, so the rolling speed decreases with passing time. Finally, this participant runs away at the same time as QGP disappearing. Therefore, the magnetic field of participant has the same life time as life time of QGP.

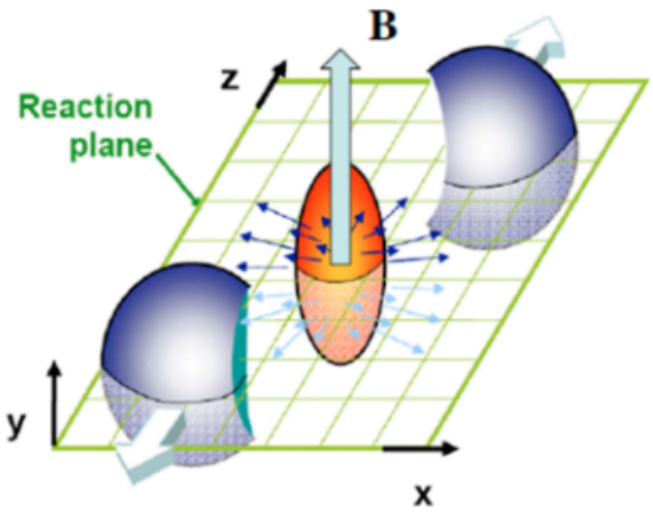

Figure 4: Generation of magnetic field [5]

1.2.1 Physics phenomenon in a intense magnetic field

In a intense magnetic field, unnormal effects occur. In this section, I describe some of these effects.

Synchrotron radiation

When a intense magnetic field is generated in QGP, quarks and anti-quarks, these are charged particles, wind the magnetic field. The winding quarks and anti-quarks lose energy with radiation of photons, gluons and leptons pair like that electrons winding a magnetic field radiate photons. In general, energy loss of quarks and anti-quarks occurs during particles pass though QGP. Therefore, this effect causes new energy loss.

Also, on synchrotron effects, radiated particles are radiated toward a tangential direction of charged particle's momentum. A magnetic field with heavy ion collisions is always generated at a perpendicular direction as reaction plane, so the radiation by the magnetic field concentrates the reaction plane and the azimuth dependence is appeared.

Photon decay and double refraction in magnetic field

In a intense magnetic field, the refraction of photon is changed by the vacuum polarization of electron-positron pair. This reason is that it is difference between the component of velocity on perpendicular and parallel with respect to a magnetic field with the anisotropy of response rate of electrons and positrons. This effect is called the vacuum double refraction.

Also, the photon with enough amount of energy can decay to the fermion and anti-fermion. This effect cannot occur in vacuum.

These effects change the refraction of perpendicular photon with respect to magnetic field. It may cause that photon yields have dependence on the azimuth.

Photon division

In the vacuum, the photon division is prohibited for Furry theorem. In a magnetic field, however, the three-point interaction occurs and it may permit to divide the photon. It permits the opposite process to this process; two low energy photons may fuse into one high energy photon. This effect can shift the photon energy distribution to milder it.

The others, the chiral magnetic effect, which the electric current flows along the parallel to a magnetic field with topological transition, and Schwinger mechanism is predicted. These are interesting and important to know physics at heavy ion collisions.

1.3 Virtual photon polarization by a intense magnetic field

The virtual photon is the photon having the mass for the uncertainty principle. The virtual photon has electron-positron loops, and finally decays to the electron and positron (Figure 5).

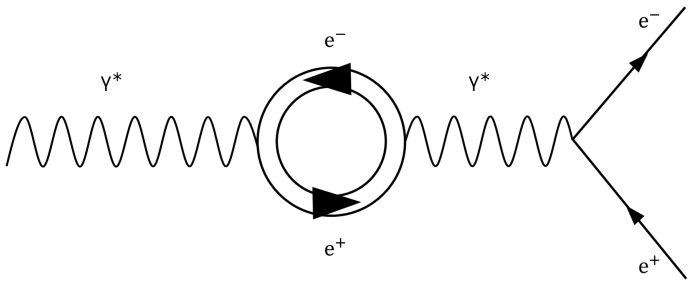

Figure 5: Diagram of virtual photon loop

If the virtual photon, it is direct photon because the life time of a magnetic field is as short as QGP, goes through a intense magnetic field, the magnetic field effects electron-positron loops of a virtual photon. A electron and positron from a virtual photon depends on the magnetic field. Therefore the detection of a virtual photon polarization proves the existence of intense magnetic field.

The degree of polarization P is defined as below equation 2.

$$P = \frac{R_{\parallel} - R_{\perp}}{R_{\parallel} + R_{\perp}}. \tag{2}$$

$R_{\parallel}$ is the probability that decays of a virtual photon is parallel to a direction of magnetic field, and $R_{\perp}$ is the probability that decays a virtual photon is perpendicular to a direction of magnetic field. The order of polarization is 10% [6].

1.4 Virtual photon in to measure the polarization

Electron-positron pairs in experimental data include the pairs from the expectation of virtual photons such as pions. Therefore a electron-positron pair from virtual photons is needed to select for the polarization measurement.

Figure 6 is the invariant mass distribution of electron pairs. The dot line shows the mass component of each particle by the cocktail simulation. The blue line is the total yield of dot lines. It is the background. The orange line is the expected direct photon mass distribution. The invariant mass distribution of Dalitz decay and direct photon is shown by Kroll-Wada formula[8].

$$\frac{1}{N_{\gamma}}\frac{dN_{e^+e^-}}{dM_{e^+e^-}} = \frac{2\alpha}{3\pi}\sqrt{1 - \frac{4m_e^2}{M_{e^+e^-}^2}}(1 + \frac{2m_e^2}{M_{e^+e^-}^2})\frac{1}{M_{e^+e^-}}S, \tag{3}$$

$$S = \begin{cases} |F(M_{e^+e^-}^2)|^2(1 - \frac{M_{e^+e^-}^2}{M^2})^3 & \text{(Hadron decay)}, \\ 1 \quad \text{(Direct virtual photon : } \mathrm{p_T} \gg \mathrm{M_{e^+e^-}}\text{)}. \end{cases} \tag{4}$$

$M_{e^+e^-}$ is the invariant mass of electron-positron pairs, m_e is the mass of electron, M is the mass of hadron, and $F(M_{e^+e^-}^2)$ is the shape factor. p_T is the transverse momentum. The orange line and blue line is normalized by the experiment data in the low mass region. Then these are fitted by r. r is the ratio of direct photon and all photon. In Figure 6, it is from the AuAu collision minimum Bias (M.B.) data, the Dalitz decay of $\pi 0$ is dominated in $M_{e^+e^-} < 120\ MeV/c^2$, and the ratio of direct photon Signal and Background (S/B) is too small. On the other hand, in $120 < M_{e^+e^-} < 300\ MeV/c^2$, the S/B ration is good.

Figure 7 is the p_T distribution of direct photon as p_T function. (a) is pp collisions data and (b) is AuAu collision data. Also the error bars and the error band represent the statistical and systematic uncertainties. Curves are expected from a Next-to-Leading-Order perturbative QCD (NLO pQCD) calculation. In this figure(b), the r is 0.15 - 0.2 in all p_T range. This value is enough large.

For the polarization measurement from a magnetic field, I use the method of J/Ψ polarization measurement. This method is discussed in details later.

1.5 Theoretical feasibility of magnetic field detection

I discuss about the estimate of theoretical feasibility of a magnetic field. The estimated for ALICE experience have already been done[6] and it is about 1σ with 2.76 TeV PbPb collisions in 2011. This value is also expected to be larger with the LHC upgrade in 2018. Hence I estimate it for PHENIX experience.

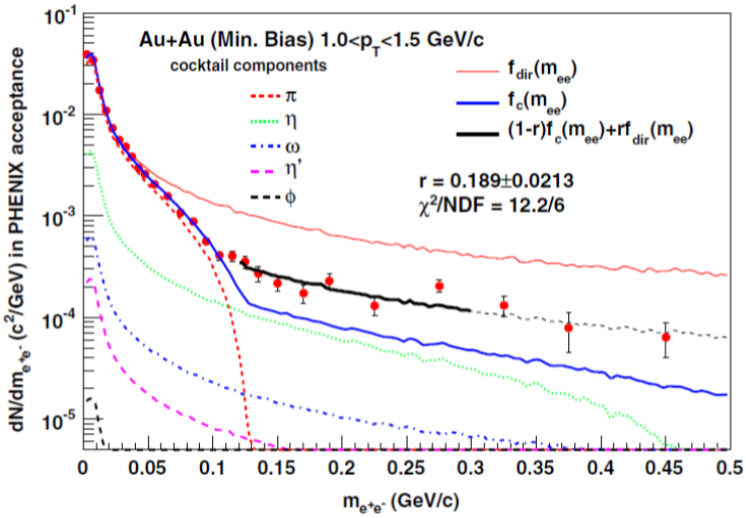

Figure 6: Invariant mass distribution of electron-positron pair for AuAu collision (M.B., $1.0 < p_T < 1.5\ GeV/c$) [7]

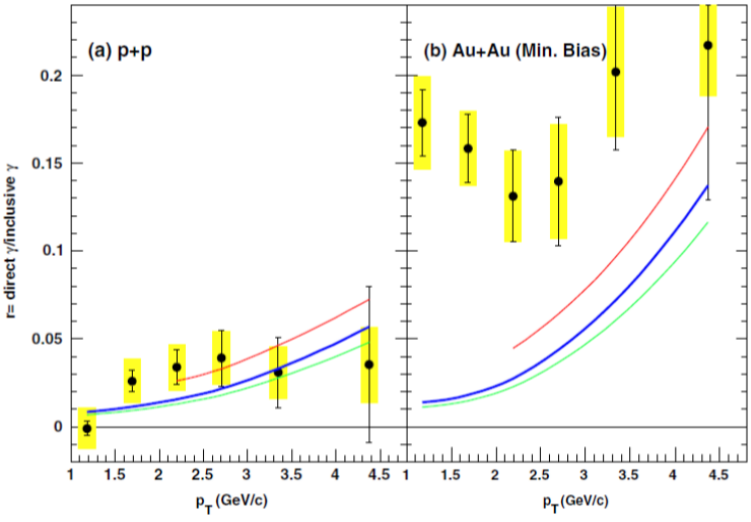

Figure 7: Fraction of the direct photon component as a function of p_T [7]

The theoretical feasibility is shown by equation 6. $N^{all}_{e^+e^-}$ is all the combinations of electron-positron pairs. These pairs include non-correlated pairs. It is called the combinatorial background B_{cb}. The ration of polarization signal S and B_{cb} is S/B_{cb}. And $f_{hadronic}$ shows the rate of electron-positron pairs from hadrons. $R_{E.P.}$ is the resolution of reaction plane, and P is the degree of virtual photon polarization. In this estimation, P is assumed to 0.1. Also the momentum of all the virtual photons is perpendicular to a magnetic field, and the polarized pattern of a virtual photon decay is perfect perpendicular or parallel to a magnetic field.

$$statistical\ significance = \frac{signal}{\sqrt{signal + background}}, \tag{5}$$

$$= \frac{N^{all}_{e^+e^-}/2 \times S/B_{cb} \times (1 - f_{hadronic}) \times R_{E.P.} \times P}{N^{all}_{e^+e^-}/2}. \tag{6}$$

The experimental data set for the estimation of theoretical feasibility is for AuAu collisions in 2004. The region of data is in $0.12 < M_{e^+e^-} < 0.3\ GeV/c^2$ and $1.0 < p_T < 2.0\ GeV/c$. Table 2 is the list of used value.

	Values
$N^{all}_{e^+e^-}$	$\sim 1.46 \times 10^5$[9]
S/B_{cb}	∼10% [9]
$f_{hadronic}$	∼80% [9]
$R_{E.P.}$	∼30% [10]
P	$O(10^{-1})$

Table 2: List of used value to estimate the theoretical feasibility

When these values are substituted, the theoretical feasibility is about 0.2σ. The M.B. event is 8.1×10^8 in 2004, on the other hand, M.B. data is 7.3×10^9 in 2010. When other conditions is the same in 2004 and 2010, the theoretical feasibility is about 0.6σ. M.B. data is larger in 2014, hence the theoretical feasibility is enough large for the detection of a magnetic field. Therefore I discuss the method of polarization measurement.

1.6 Purpose

The detection of a intense magnetic field is much important to understand physics effects at heavy ion collisions. In this thesis, I discuss the feasibility of a magnetic field detection and evaluate the detection method using the J/Ψ polarization measurement. For evaluation, I divide the polarization case into the non-polarization, perpendicular polarization and parallel polarization with respect to the magnetic field, then compare results using the methods detecting polarization of each case. Then I simulate the photon polarization to conclude that the method gives the most different result by different polarization scenarios, in short, to decide the most useful method.

2 Experiment

In this study, effects of detectors at relativistic heavy ion collision experiments are considered. I discuss that two detector in this thesis, PHENIX and ALICE detector. These are shown in this section.

2.1 RHIC accelerator

Relativistic Heavy Ion Collider (RHIC) at BrookHeaven Natioal Laboratory (BNL) to the fundamental study for relativistic heavy ion collisions. It is composed by double ring (blue ring and yellow ring), and the circumferential length of its is about 3.8km. This accelerator is the first relativistic heavy ion collider and it specializes in the heavy ion acceleration. Therefore it can accelerate many types of atoms such as U, Au, Al, He3 and deuterium. It means that this accelerator can verify many physic phenomenons which generated by heavy ion collisions. RHIC accelerator can accelerate a proton to 250 GeV and a heavy ion to 100GeV per nucleon.

RHIC has 4 experiment: PHENIX, STAR, BRAHMS, PHOBOS. I focus PHENIX experience in this thesis.

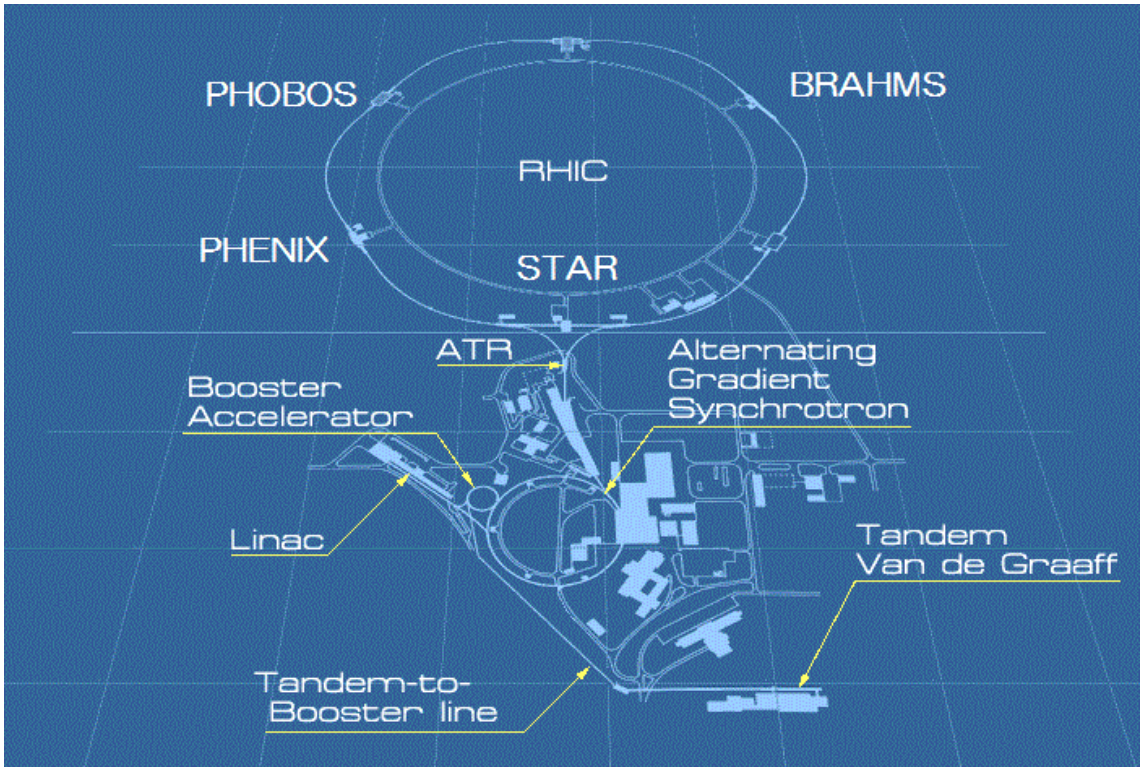

Figure 8: RHIC accelerator [11]

2.1.1 PHENIX experiment

The purpose of PHENIX experiment is the generation of QGP and the elucidation of QGP characterization. This experience is with 430 scientists, 11 countries and 43 organizations.

From Japan, The University of Tokyo, University of Tsukuba, Hiroshima University and RIKEN are participated. PHENIX experiment specializes in the measurement of photons and leptons, so it is very suitable for the measurement of polarized photons. The Figure 9 is the overview PHENIX detector.

The PHENIX detector is separated as bellow.

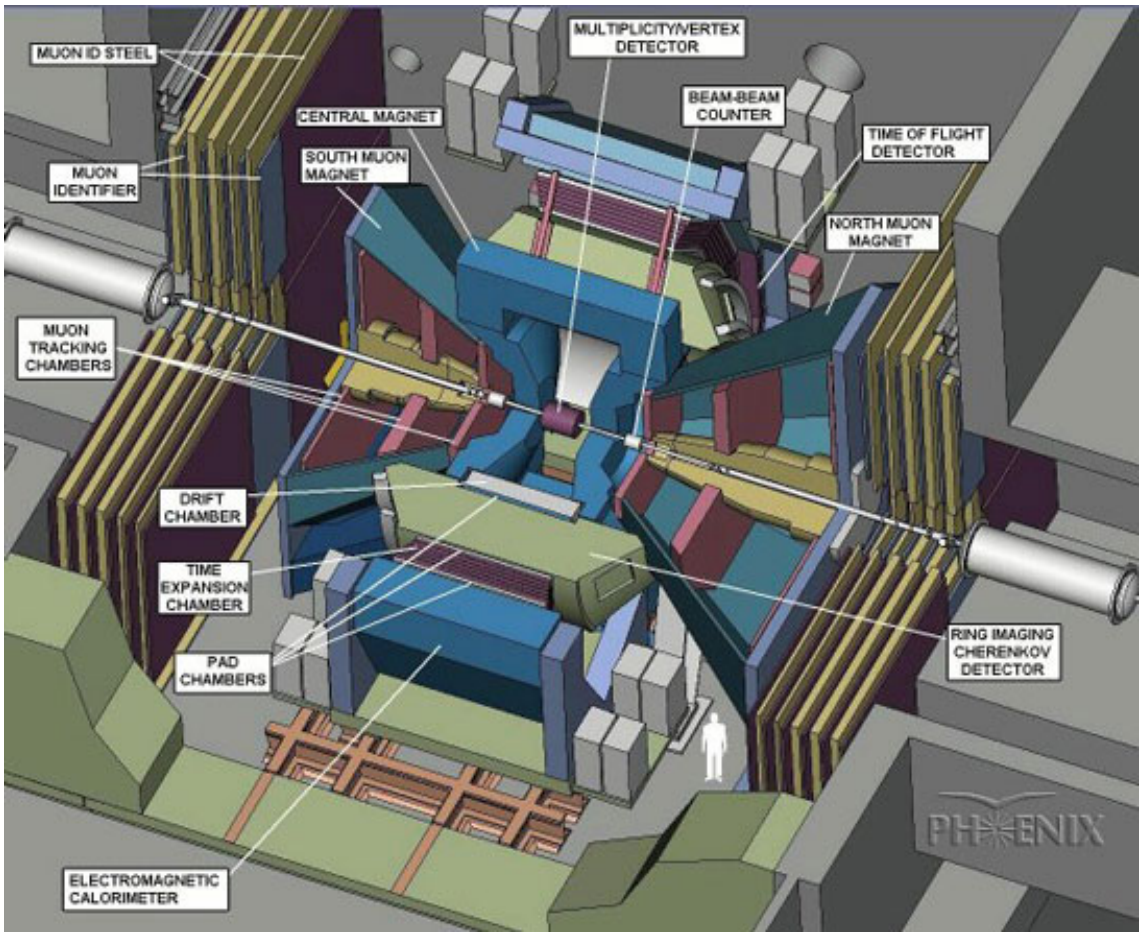

Figure 9: PHENIX detector [12]

1. Central Arm detector (-0.35 $< \eta <$ 0.35)

   The Central Arm detector, that is divided into East Arm and West Arm, measures momentums and tracks of charged particles. Also charged particles are identified by it.

2. Muon Detector (-2.45 $< \eta <$ -1.15, 1.15 $< \eta <$ 2.44)

   The Muon Detector measures forward muons. Muons is the lepton which does not interact with QGP by the strong force. Therefore the measurement of muons is importance to get the information about the initial state.

3. Grovel detector (3.4 $< |\eta|$)

   The Grovel detector triggers the measurement of events. This detector measures the the centrality, luminosity, collision timing and collision point.

2.1.2 PHENIX detectors

I introduce some PHENIX detectors to measure the polarized photon detector below.

Electro Magnetic Calorimeter (EMC)

EMC measures the energy and potential of photons and charged particles. It covers the pseudo rapidity $< \eta < 0.375$, and azimuth $30° < |\phi| < 120°$. In EMC, charged particles generate photons by the bremsstrahlung. These photons generate electrons and positrons by the electron-positron pair generation, then these electrons and positrons generate photons. This process, it is called the electro-magnetic shower, is repeated until energy is under the critical energy point of electron-positron pair. EMC detects the energy from this process and reconstructs generated particles.

EMC is composed by the lead scintillator (PbSc) calorimeter and lead glass (PbGl) calorimeter. PbSc is at four sectors in the West Arm, and PbSc is at two sectors and PbGl sectors is at two sectors in the East Arm.

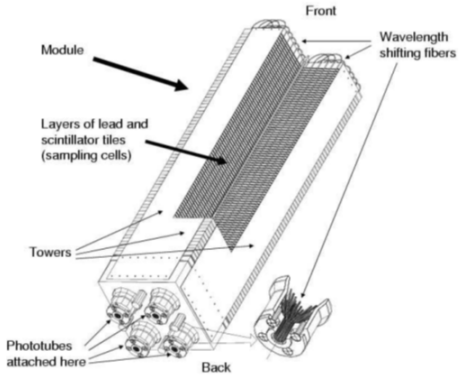

EMC of lead-scintillator module [13]

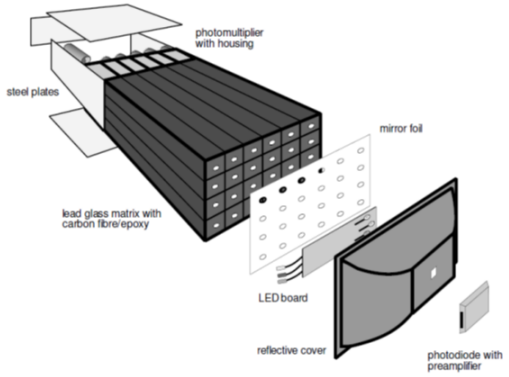

EMC of lead-glass super module [13]

Figure 10: EMC detector

Ring Imaging CHerenkov counter (RICH)

RICH identifies charged particles. The speed of particle is difference by each mass in the medium. Also, charged particles in the medium scat the light when the speed of these is greater then the speed of light in the medium. The radiation angle θ of this scattering light, it is called Cherenkov light, is $cos\theta = 1/n\beta$. Hence the measurement of radiation angles informs the mass of charged particle, therefore charged particles are identified. The medium gas (radiator gas) in RICH is CO_2, and RICH detects the radiation light by Photon Multiplier Tubes (PMT). Also it covers the pseudo rapidity $|\eta| < 0.35$ and azimuth $30° < |\phi| < 120°$.

DCH (Drift CHamber)

DCH, this wire chamber covers both the Central Arms, is the main detector for tracking charged particles. It covers the pseudo rapidity $|\eta| < 0.7$, and azimuth $-34° < \phi < 56°$ on the west central arm and azimuth $125° < \phi < 215°$ on the east central arm. This detector measures tracks of charged particles by connecting detect

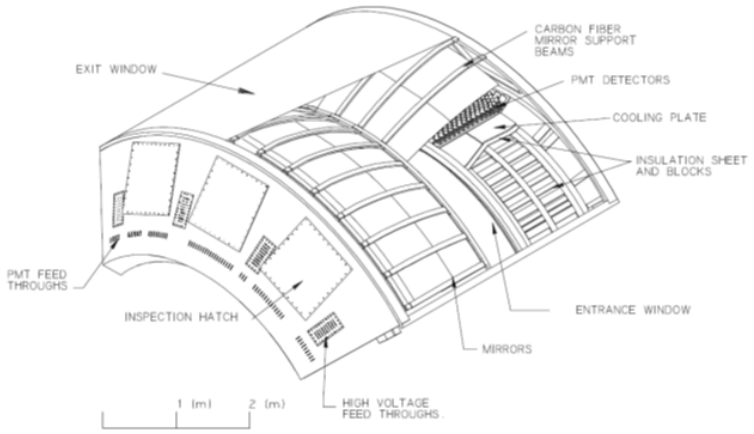

Figure 11: RICH detector [14]

points of charged particles which are bended tracks by the artificial magnetic field. Also the transverse momentum is reconstructed by the measurement of curvature of charged particle's track.

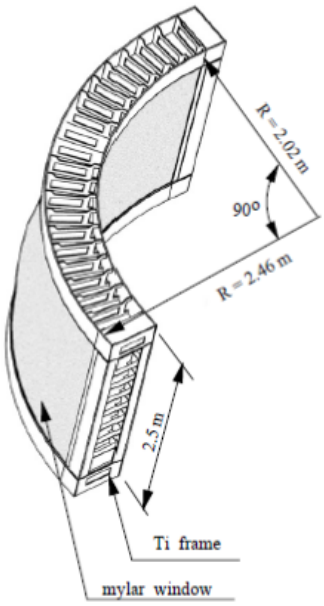

Figure 12: DCH detector [15]

2.2 LHC accelerator

Large Heavy ion Collider (LHC) is at European Organization for Nuclear Research (CERN). It is at about 100m underground, and the circumferential length of its is about 27km. This accelerator started up on 2008 with over about 10,000 scientists and about 100 countries and organizations. Also LHC is the largest collider in the world, and it can accelerate the proton beam to 7.0 TeV. This accelerated energy is also the highest in the world.

LHC have 6 experiment: ATLAS, CMS, ALICE, LHC-b, TOTEM, LHC-f. These experiments have difference purpose and difference detector for each purpose. For example, the purpose of ATLAS and CMS is the discovery of Higgs boson, generation of dark matter (supersymmetric particle: SUSY) and the consideration of beyond standard model. In this thesis, I discuss the ALICE experience for relativistic heavy ion collision.

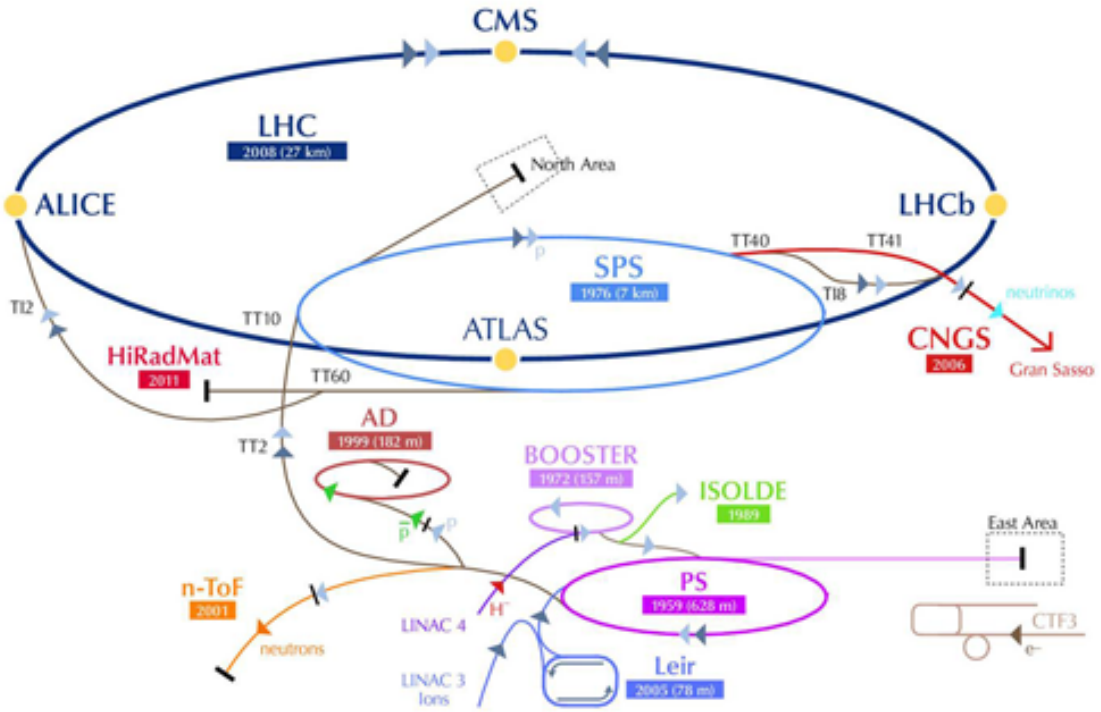

Figure 13: LHC accelerator [1]

2.2.1 ALICE experience

ALICE experience is an abbreviation of "A Large Ion Collider Experiment". The purpose of ALICE experience is the generation of QGP with PbPb collisions and the elucidation of QGP characterization. This experience is with 1,300 scientists, 35 countries and 120 organization. The University of Tokyo, University of Tsukuba, Hiroshima University and RIKEN are collaborated from Japan. This experience only specializes in measure relativistic heavy ion collisions at LHC experience. Therefore ALICE detector is needed to detect many physics phenomenon which is generated with heavy ion collisions into wide energy area. The Figure 14 is the overview of ALICE detector.

The ALICE detector is separated as bellow.

1. Central Barrel (-0.9 $< \eta <$ 0.9)

   The Central Barrel covers near the collision point. It is in the dipole magnet for applying 5,000 Gauss. This magnetic field bends charged particles generated by heavy ion collisions, and momentums of these particles can be measured.

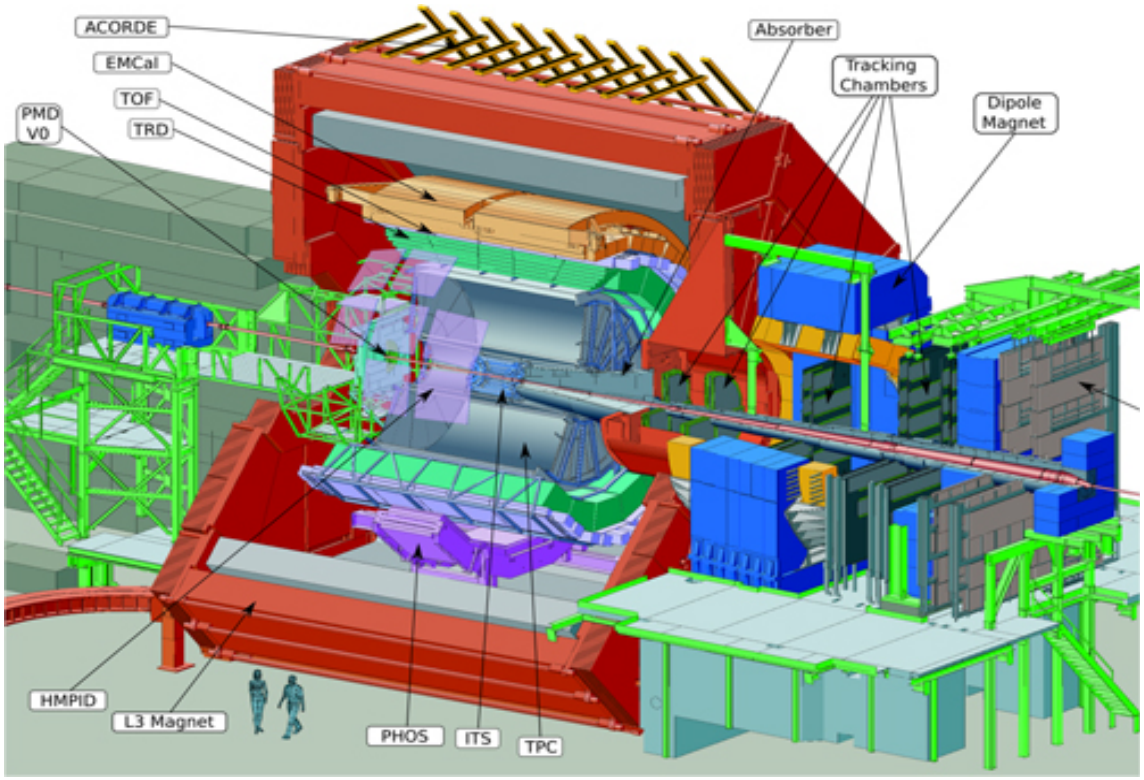

Figure 14: ALICE detector [1]

2. Dimuon Spectrometer (-4 $< \eta <$ 2.5)

   The Dimuon Spectrometer measures the forward muon. The muon measurement is important as with PHENIX.

3. Grovel detector (3.4 $< |\eta|$)

   The Grovel detector selects collision events like PHENIX. For this selection, the centrality, luminosity, collision timing and collision point is known.

2.2.2 ALICE detectors

I introduce some ALICE detectors to measure the polarized photon like PHENIX detector below.

Inner Tracking System (ITS)

ITS is at nearest the beam collision point. It covers the pseudo rapidity $-0.9 < \eta < 0.9$ and azimuth 2π. This detector measures tracks of charged particles and energy loss per a unit length (dE/dx). Also it can measure the number, collision point and decay point of particles. The identification of particle species is decided using it.

ITS consists of SPD (Silicon Pixel Detector), SDD (Silicon Drift Detector) and SSD (Silicon Strip Detector). SPD is the innermost two layers, SSD is the following two layers, and SPD is the two outer layers. These are the front line of silicon detector.

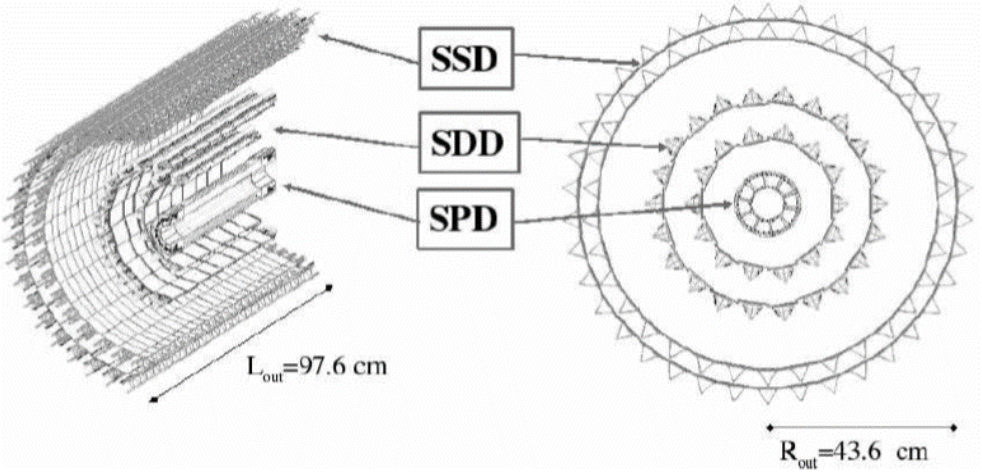

Figure 15: ITS detector [16]

Time Projection Chamber (TPC)

TPS is the wire chamber at 85-250cm from the beam collision point. This detector is much superior to measure tracks of charged particles and dE/dx, and the main detector to measure charged particles. It covers the pseudo rapidity $-0.9 < \eta < 0.9$ and azimuth 2π. The mixed gas (Ne/CO2/N2 : 85.7%/9.5%/4.8%) fills in this detector. Energy loss and ion pair generation by ionization with charged particles occur passing through this gas. Generated ionize electrons are drifted by inner electric field, then tracks of charged particles are reconstructed using the position and time information of this electron. Also, for measurements of charged particles dE/dx, it can identify particle species.

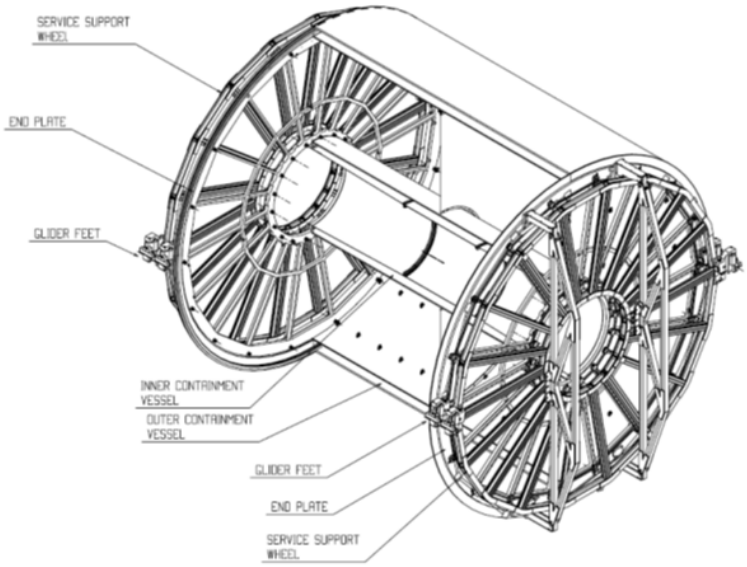

Figure 16: TPC detector [16]

Time of Flight (TOF)

TPC measures the flight time of charged particles. The flight time is different for each particles, so particles are identified by the combination of the flight distance, the momentum and the flight time. It has the high time resolution, about 50ps, it means that it can divide particles which has the momentum 1.5GeV/c to kaon and pion.

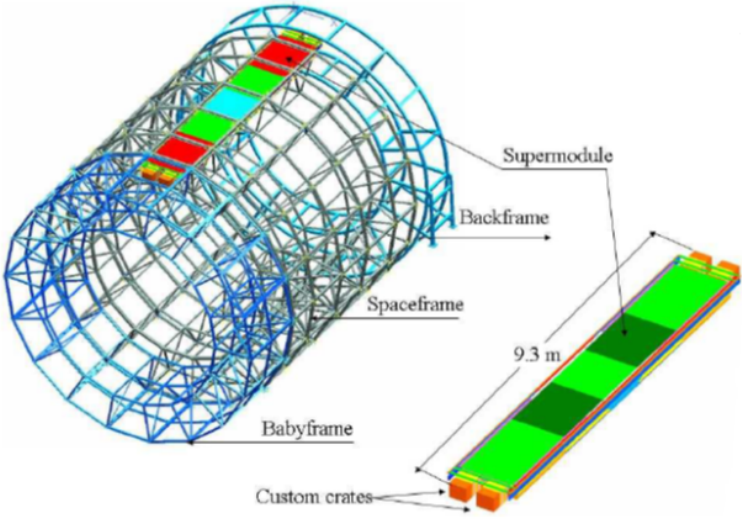

Figure 17: TOF detector [16]

3 Method

To measure polarized photons, I use below three polarization frames. These frames are used to observe the J/ψ polarization. In this section, features of these frames are described.

3.1 Definition of polarization frames

This method is the measurement on the frames which are defined by the decayed leptons pair (in this thesis, electron and positron) from the polarized particle (in this thesis, virtual photon). The frames are called "Helicity (HX) frame", "Gottfried-Jacson (GJ) frame" and "Collins-Soper (CS) frame". All the frames is on the rest frame of the leptons pair. Also, all the frames is the same frame when the velocity of polarized particles is zero. To use three polarization frames, x, y and z axis should be defined. The belows are the definition of z axis in each polarization frames (Figure 18, [17]). In these plot, y axis is the perpendicular axis to production plane including z axis and collision beams. y axis is the same on all polarization frames. x axis is defined as y axis and z axis on right-handed system in each polarization frames.

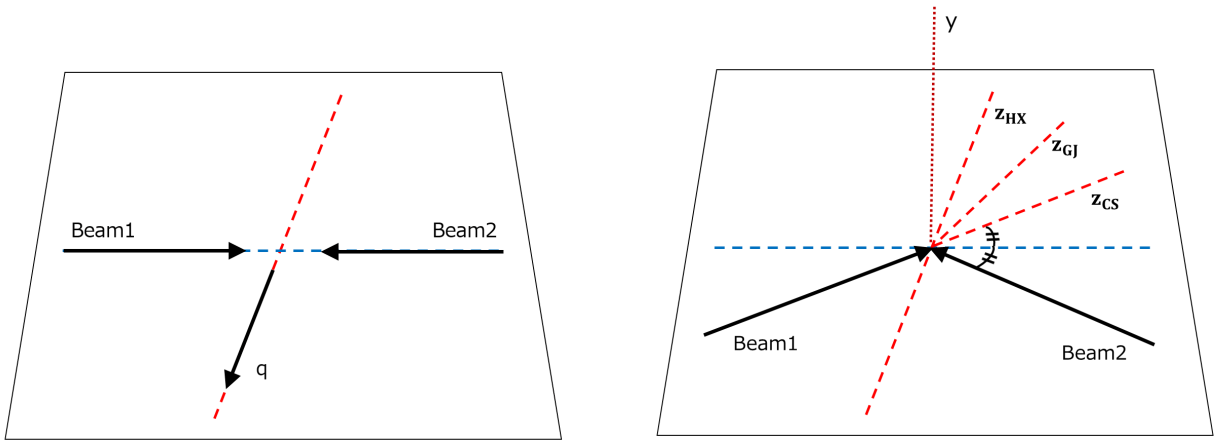

collisions center of mass frame q rest frame

Figure 18: Polarization frames

3.1.1 Feature of each polarization frame

1. Helicity (HX) frame

   z axis is that the momentum direction of leptons pair on the laboratory system.

   The direction of magnetic field is always the vertical direction to the reaction plane 4. Also the reaction plane is the vertical plane to the beam axises. Thus the momentum direction of the polarized particle, this particle is the parent particle which decays into leptons pair, to the magnetic field direction depends on the beam axises, that is z axis on the laboratory system.

On HX frame, the polarization is measured by observing the momentum correlation between the decayed positive lepton and the polarized parent particle. The purely momentum polarization from magnetic field effect can be measured on this frame.

However, The polarization measurement on HX frame just only uses the correlation between the momentum direction of decayed lepton and parent particle. Hence the momentum deviation except from a magnetic field effect, such as miss reconstruction, is too effective.

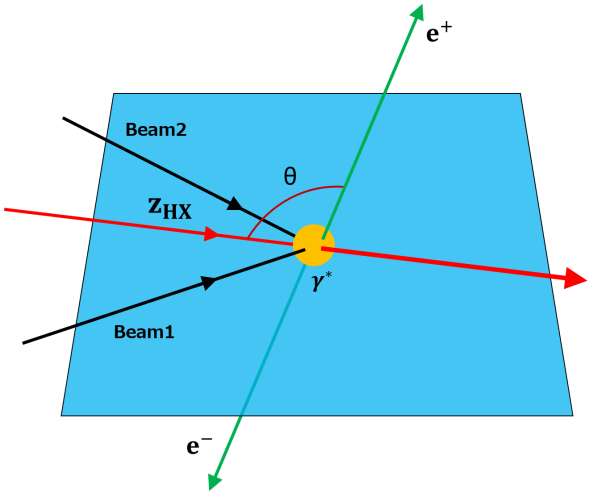

Figure 19: Definition of HX frame on lepton pair rest frame

2. Gottfried-Jackson (GS) frame

   z axis is that the beam momentum (beam1 or beam2 in Figure 18) on the rest frame of leptons pair.

   On GS frame, the polarization is measured by observing the correlation between a beam axis and the positive lepton. It reflects the correlation between a beam axis, it is the vertical axis to the direction of magnetic field, and the polarized particle. Also, the zx plane and y axis on the laboratory system and on GS frame is the same when the transverse momentum of parent particle is enough small.

   However, this frame is defined by using only one of two beam axises. This encompasses the weakening of the correlation between magnetic field direction and polarized particle, because the direction of a magnetic field is vertical to the both beam axises. This effect is more effective when the the transverse momentum of parent particle is not neglected, in other wards, the both beam axises on the laboratory system and on GJ frame is not on the same plane.

3. Collins-Soper (CS) frame

   z axis is that the bisector of beams (beam1 and -beam2 or -beam1 and beam2 in Figure 18) on the rest frame of leptons pair.

   On CS frame, the polarization is measured by observing the correlation between the both beam axises and the positive lepton. The effect of momentum direction

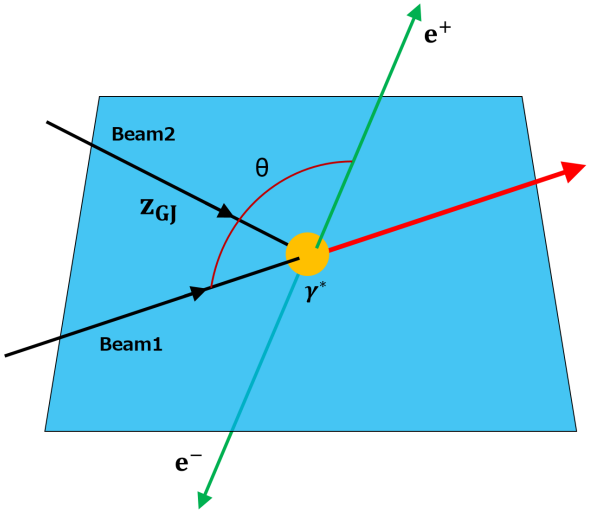

Figure 20: Definition of GJ frame on lepton pair rest frame

of polarized parent particle is small on this frame. The zx plane and y axis on this frame, on the laboratory system and on GJ frame is the same when the transverse momentum of parent particle is neglected. And CS frame is rotated by 90° around y axis when the transverse momentum of parent particle is enough high and the longitudinal momentum is neglected.

However, this frame uses two beam axises. Hence the correlation between the parent particle and the beam axises is weaker than other frames.

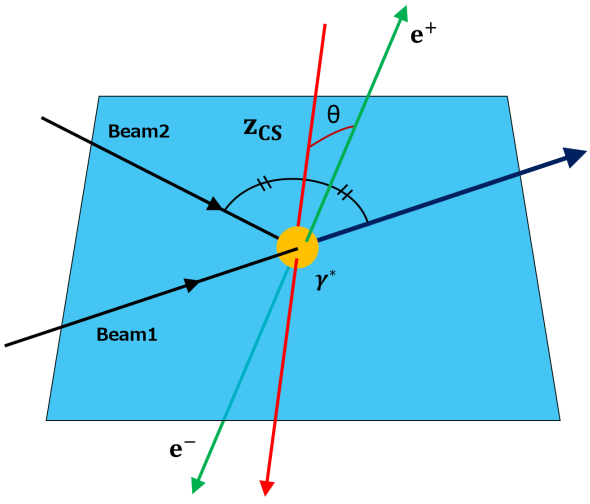

Figure 21: Definition of CS frame on lepton pair rest frame

These frames have the advantage and disadvantage. Therefore the good frame selection as measured target is needed.

3.1.2 Definition of angle on polarization frame

The zenith angle θ is defined as the angle between z axis and the angle of positive charged lepton. The azimuth angle is defined as the angle between x axis and the vector of positive charged lepton projected on xy plane (Figure 22).

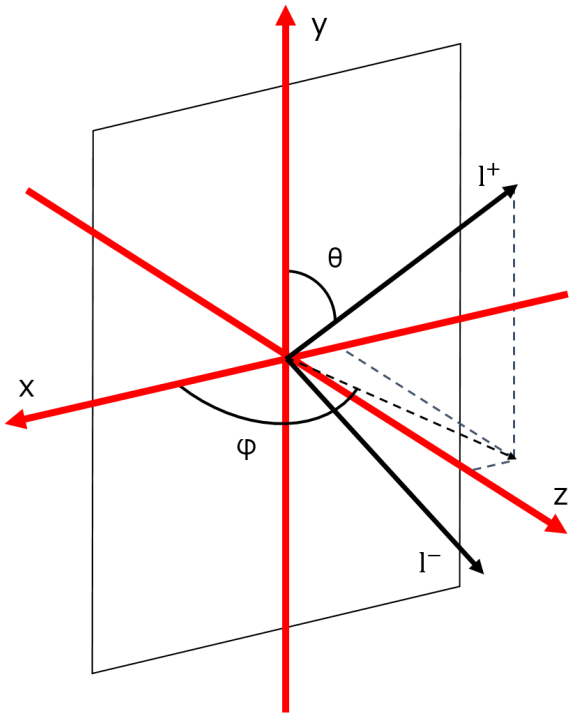

Figure 22: Definition of zenith angle and azimuth angle

3.2 Calculation of polarization parameter

The angle distribution $W(cos\theta, \phi)$ of polarized event is the below equation 8. i is the contributing production processes andf^i is the weighting function.

$$W(cos\theta, \phi) = \sum_{i=1}^{n} f^{(i)} W^{(i)}(cos\theta, \phi), \tag{7}$$

$$\propto \frac{1}{3+\lambda_\theta}(1 + \lambda_\theta cos^2\theta + \lambda_\phi sin^2\theta cos\phi + \lambda_{\theta\phi} sin2\theta cos\phi). \tag{8}$$

Also, The each angle distribution can be calculated to integrate equation refeq:W over $cos\theta$ and ϕ (equation 9, 10).

$$W(cos\theta) \propto 1 + \lambda_\theta cos^2\theta, \tag{9}$$

$$W(\phi) \propto 1 + \frac{2\lambda_\phi}{3+\lambda_\theta} cos^2\theta. \tag{10}$$

$\lambda_{\theta,\phi,\theta\phi}$ is the polarization parameter. To calculate $\lambda_{\theta\phi}$, the below definition (equation 12) of $\tilde{\phi}$ is needed. The equation of $\tilde{\phi}$ distribution is shown by equation 11. If the $\tilde{\phi}$ is out from 0 to 2π, the $\tilde{\phi}$ is needed to properly add or subtract the 2π to become $0 < \tilde{\phi} < 2\pi$. The $\lambda_{\theta\phi}$ is calculated by it.

$$\tilde{\phi} \propto \begin{cases} \phi - \frac{3}{4}\phi(cos\theta < 0), \\ \phi - \frac{1}{4}\phi(cos\theta > 0). \end{cases} \tag{11}$$

$$W(\tilde{\phi}) \propto 1 + \frac{\sqrt{2}\lambda_{\theta\phi}}{3+\lambda_\theta} cos\tilde{\phi}. \tag{12}$$

These polarization parameters show the asymmetry of the number of particles on angle distribution. Therefore, these parameters can be shown by the below equation 15. $P(|cos\theta|)$ is the probability distribution of positive charged lepton.

$$\frac{P(|cos\theta| > 1/2) - P(|cos\theta| < 1/2)}{P(|cos\theta| > 1/2) + P(|cos\theta| < 1/2)} = \frac{3}{4}\frac{\lambda_\theta}{3+\lambda_\theta}, \tag{13}$$

$$\frac{P(|cos2\phi| > 0) - P(|cos2\phi| < 0)}{P(|cos2\phi| > 0) + P(|cos2\phi| < 0)} = \frac{2}{\pi}\frac{2\lambda_\phi}{3+\lambda_\theta}, \tag{14}$$

$$\frac{P(|sin2\theta cos\phi| > 0) - P(|sin2\theta cos\phi| < 0)}{P(|sin2\theta cos\phi| > 0) + P(|sin2\theta cos\phi| < 0)} = \frac{2}{\pi}\frac{2\lambda_{\theta\phi}}{3+\lambda_\theta}. \tag{15}$$

λ_θ is shown by the anisotropy of zenith angle. Therefore $\lambda_\theta = 0$ is no-polarization, $\lambda_\theta > 0$ is parallel polarization and $\lambda_\theta < 0$ is perpendicular polarization (Figure 23).

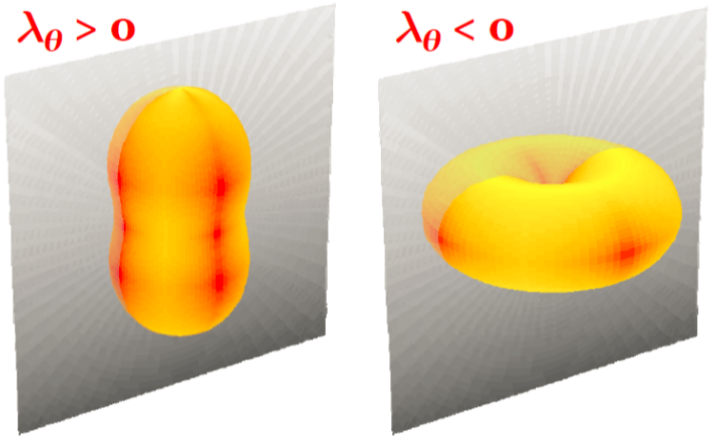

Figure 23: Aanisotropy of zenith angle [18]

λ_ϕ is shown the anisotropy of azimuth angle. Therefore $\lambda_\theta = 0$ is no-polarization, $\lambda_\theta > 0$ is parallel polarization and $\lambda_\theta < 0$ is perpendicular polarization (Figure.24).

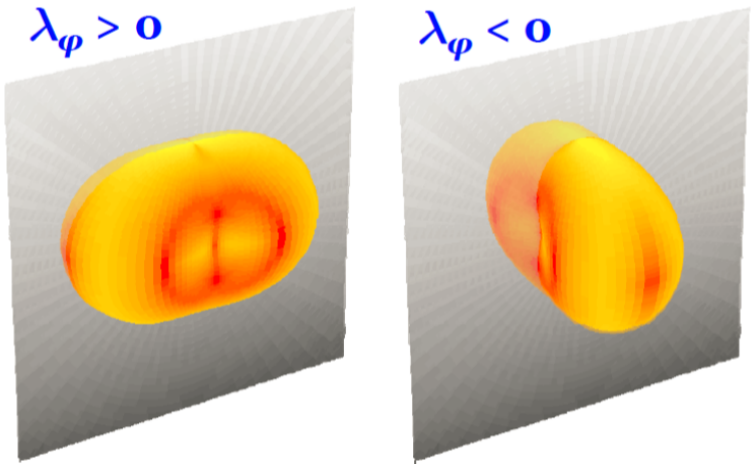

Figure 24: Anisotropy of azimuth angle [18]

Also, $\lambda_{\theta\phi}$ is used to define the "better" polarization frame. The "best polarization frame" is that $\lambda_{\theta,\phi}$ have the best significance and the symmetry is the most shape. The degree of symmetry is expressed by δ and this equation is below (equation 16).

$$\delta = \frac{1}{2} arctan(\frac{2\lambda_{\theta\phi}}{\lambda_\phi - \lambda_\theta}). \tag{16}$$

δ shows the angle of rotation around y axis. The polarization frame having most small δ is the most symmetric shape (Figure 25). In this figure, x'y'z' system is good frame. xyz system deviate delta from x'y'z' system.

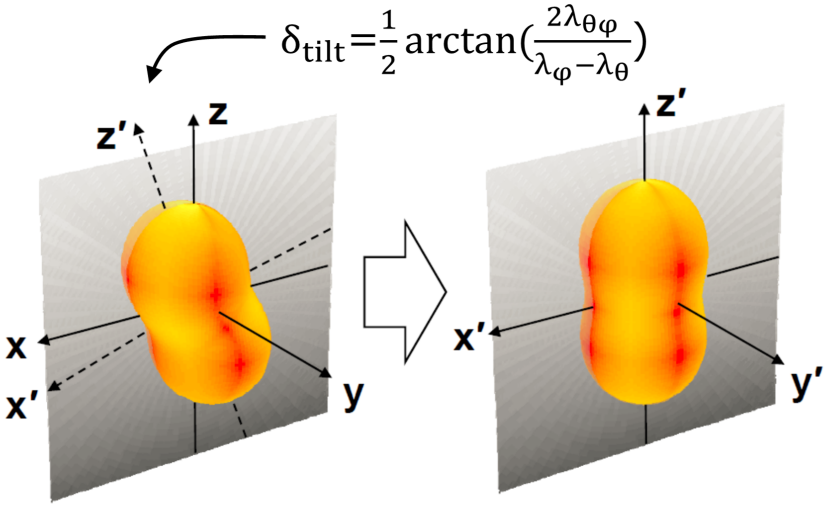

Figure 25: Deviation from good frame [18]

4 Simulation

4.1 Method of simulation

To think the polarization, I thought in the three cases that virtual photons have no-polarization, perpendicular polarization and parallel polarization with respect to a magnetic field (Figure 26).

Also, to estimate the precise polarization parameter, the background estimation is needed. I used Heavy Ion Jet INteraction Generator (Hijing) to estimate the back ground. Hijing is Monte Carlo simulation to simulate the pp and AA collision. This generator reproduce the heavy ion collision events which have the jet correlation and the no-polarization. Therefore it is suitable to estimate the background for this simulation. The particles in events that is generated by Hijing have the jet correlation. Also, particles which is generated by Hijing is combined to reconstruct parent particles and reproduce physics phenomena from heavy ion collisions. The event having the correlated particles is called "same Hijing event" in the following, because the correlated particles is combined in the same collision event. Also, the event having the non-correlated particle is called "mixed Hijing event" in the following. Because the no-correlated particles is reconstructed the combination of particles in the different collision events, in other words, the different events is mixed.

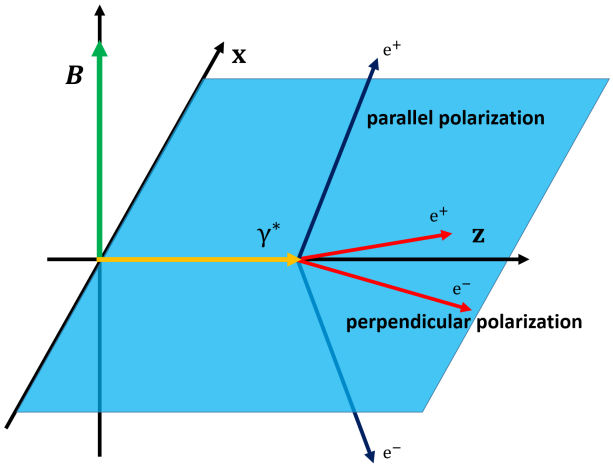

Figure 26: Polarized lepton pair as polarization case

4.2 Hijing event

The Hijing events includes electron pairs from the expectation of virtual photons, I limit the invariant mass and transverse momentum. In this thesis, the limit of reconstructed pair is $0.12 < M_{e^+e^-} < 0.3\ GeV/c^2$ and $1.0 < p_T < 5.0\ GeV/c$.

4.2.1 Same Hijing simulation

The cosθ distribution of positron in same Hijing event is Figure 27.

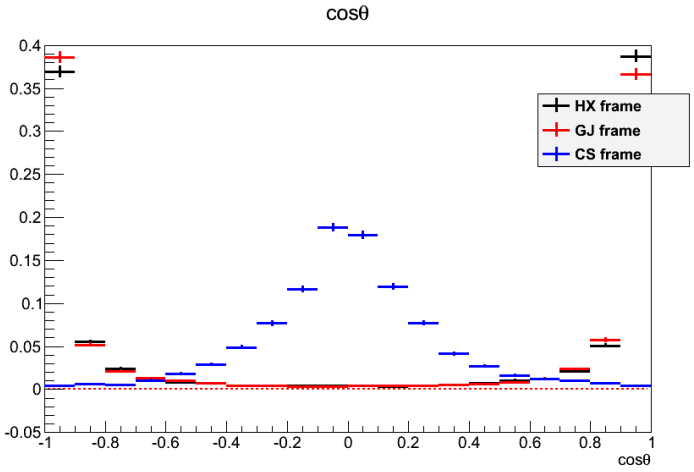

Figure 27: $cos\theta$ distribution by Same Hijing event

This cosθ distribution is normalized by entry, so this shows the probability distribution of positron. This distribution has the correlation. This reason is that when the high p_T particle exists, the pair in cut region is reconstructed with one high p_T particle and many low p_T particle that is near the high p_T particle (Figure 28). Hence the opening angle between high p_T particle and low p_T particle is small. Therefore the deviation on the plot is appeared.

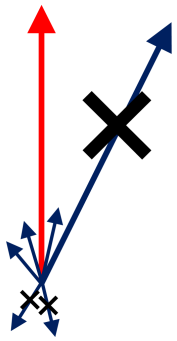

Figure 28: Image of p_T selection in cut region [7]

4.2.2 Mixed Hijing simulation

To reject the correlation expect from the polarization of magnetic field effect, I use the mixed Hijing events. This mixed Hijing events also shows the probability distribution of positron by normalization like the same Hijing events. The cosθ distribution, it is subtracted the cosθ distribution of the mixed Hijing events from the cosθ distribution of the same Hijing event, is Figure 29, and the λ_θ from this cosθ distribution is Figure 30. The λ_θ is zero within uncertainties. It means that the λ_θ becomes zero on all the frames when the case is no-polarization.

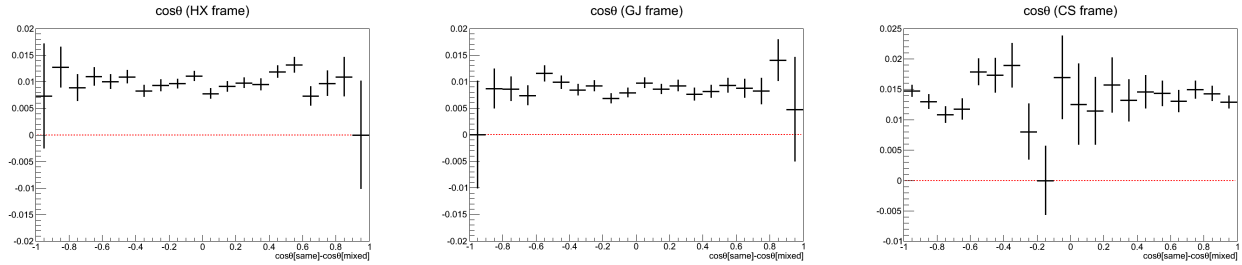

$cos\theta$ distribution on HX frame $cos\theta$ distribution on GJ frame $cos\theta$ distribution on CS frame

Figure 29: $cos\theta$ distribution as each polarization frames

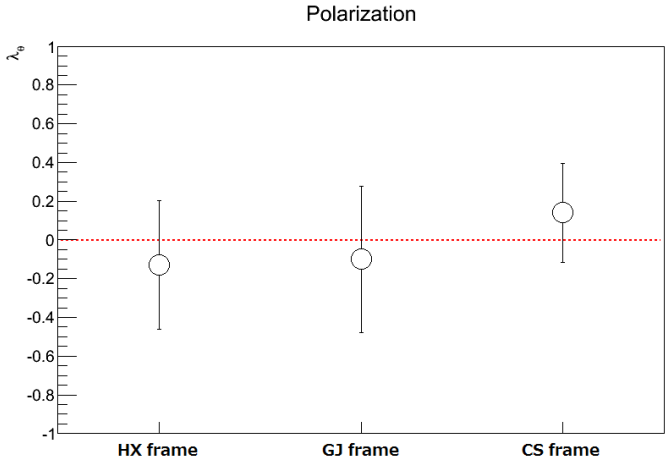

Figure 30: λ_θ of Hijing event

4.3 Signal event

I created the electron and positron from virtual photon by myself, then the electron and positron are polarized depending on three polarization cases. This polarized electron-positron pair is called "signal event". The cosθ distribution is Figure 31. All the simulated electron pairs have the polarization. cosθ distribution is obvious difference as each different polarization. I mix this signal event to the same Hijing event. When particles is reconstructed by combining the same event to reconstruct the reproduce physics phenomena like the same Hijing event, this events is called "same signal-Hijing event". Also, when particles is reconstructed by combining the different events like the mixed Hijing event, this events is called "mixed signal-Hijing event"

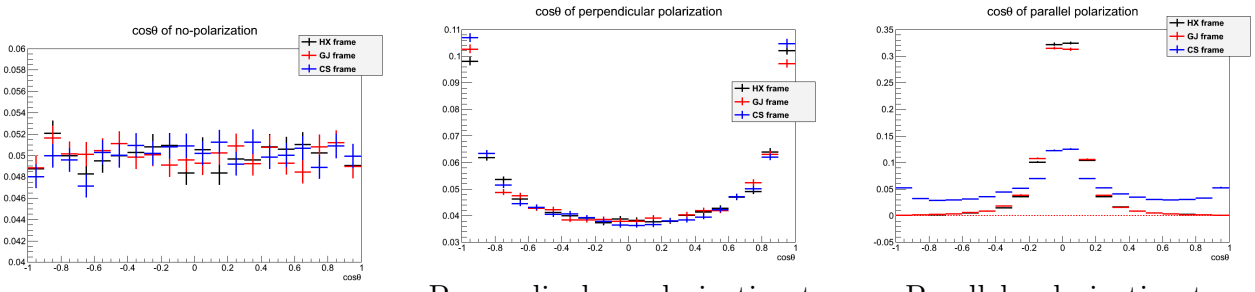

No-polarization | Perpendicular polarization to magnetic field | Parallel polarization to magnetic field

Figure 31: *cosθ* distribution of signal as each polarization case

4.4 Signal-Hijing event

The cosθ distribution by same signal-Hijing event is Figure 32. In this distribution, the parallel polarization can be distinguished from no-polarization and perpendicular polarization. In contrast, the perpendicular polarization can not be distinguished from no-polarization. This reason is that the shape of cosθ distribution of signal event, that is perpendicular polarization, and the same Hijing event is almost the same.

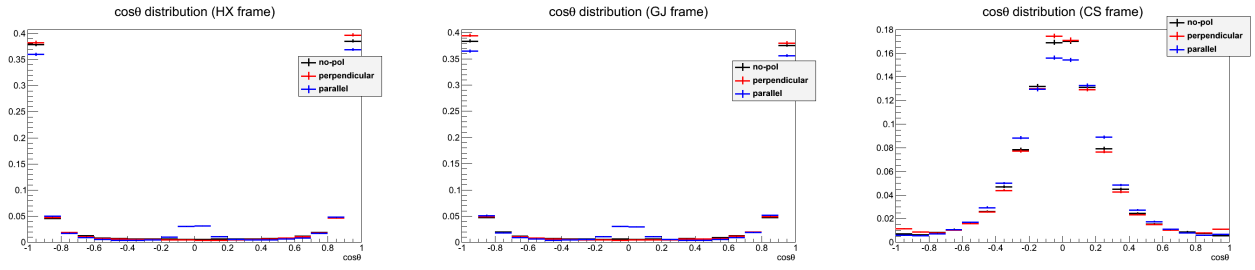

cosθ distribution on HX frame | *cosθ* distribution on GJ frame | *cosθ* distribution on CS frame

Figure 32: *cosθ* distribution on each polarization case

4.5 Subtraction of background effect

To emphasize the difference of cosθ distribution for each polarization case, the normalized cosθ distribution of mixed signal-Hijing event is subtracted from the normalized cosθ distribution of same signal-Hijing event. This result is Figure 33.

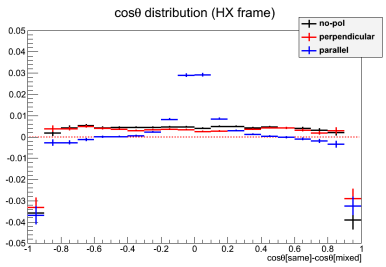

Subtracted *cosθ* distribution on HX frame

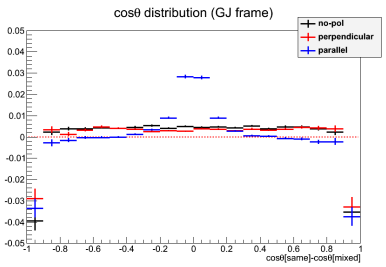

Subtracted *cosθ* distribution on GJ frame

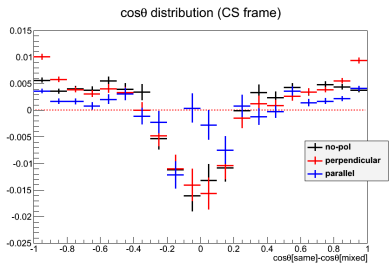

Subtracted *cosθ* distribution on CS frame

Figure 33: Subtracted *cosθ* distribution on each polarization case

By this subtraction, the probability distribution of positron is negative on some region. Hence I correct the cosθ distribution so that the smallest value is 0 (Figure 34). The cosθ distribution means only the deviation of positron distribution, so this correction influence the deviation from polarization.

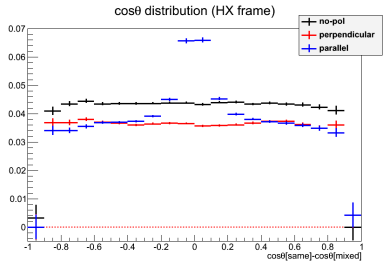

Corrected *cosθ* distribution on HX frame

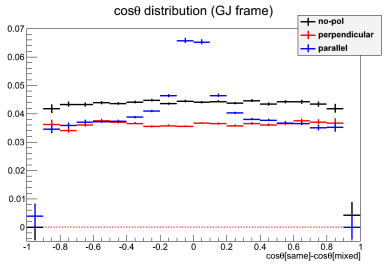

Corrected *cosθ* distribution on GJ frame

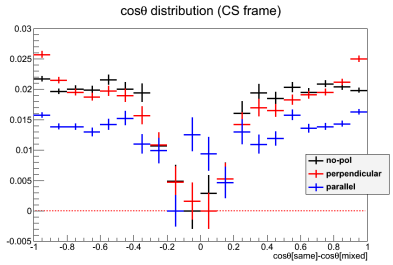

Corrected *cosθ* distribution on CS frame

Figure 34: Corrected *cosθ* distribution on each polarization case

5 Result

5.1 Selection of good frame

The $\lambda_\theta, \lambda_\phi$ and $\lambda_{\theta\phi}$ is Table 3 and Figure 35. The used event set is that one polarized pair is in one collision event for the purpose that the polarization influence is more effective to select the best frame. Also the acceptance covers all region. The number of event is 10,000.

polarization case	polarization frame	λ_θ	λ_ϕ	$\lambda_{\theta\phi}$
no-polarization	HX frame	-0.40 ± 0.032	-0.26 ± 0.018	0.005 ± 0.022
	GJ frame	-0.40 ± 0.032	-0.19 ± 0.015	-0.26 ± 0.015
	CS frame	1.7 ± 0.17	-0.27 ± 0.012	0.06 ± 0.089
perpendicular	HX frame	-0.35 ± 0.039	0.81 ± 0.025	-0.01 ± 0.015
	GJ frame	-0.35 ± 0.039	0.79 ± 0.026	-0.21 ± 0.014
	CS frame	2.4 ± 0.22	-0.24 ± 0.025	-0.07 ± 0.089
parallel	HX frame	-0.69 ± 0.031	-0.42 ± 0.015	0.013 ± 0.025
	GJ frame	-0.68 ± 0.031	-0.41 ± 0.013	-0.27 ± 0.032
	CS frame	1.0 ± 0.17	-0.41 ± 0.018	-0.003 ± 0.039

Table 3: List of $\lambda_\theta, \lambda_\phi$ and $\lambda_{\theta\phi}$ at all acceptance

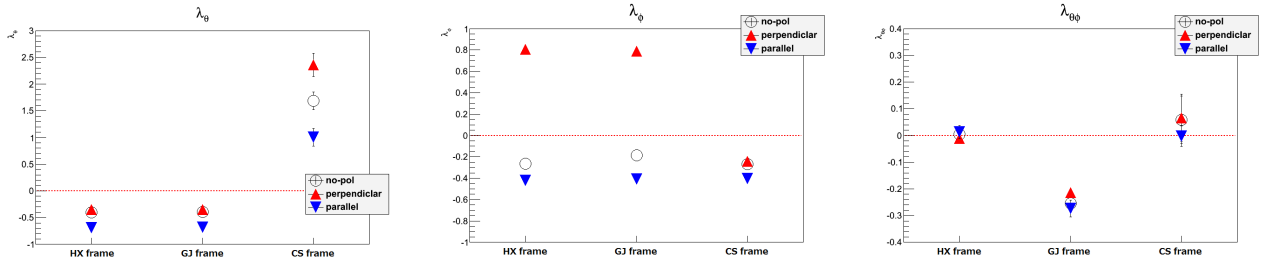

λ_θ λ_ϕ $\lambda_{\theta\phi}$

Figure 35: $\lambda_\theta, \lambda_\phi$ and $\lambda_{\theta\phi}$ at all acceptance

In this figure, the λ_θ value is the same on HX frame and on GJ frame when the polarization case is the no-polarization and the perpendicular polarization. And when the case is the parallel polarization, λ_θ is nearly the other value on HX frame and on GJ frame. On the other hand, λ_θ on CS frame is the enough different for each polarization cases. Also, λ_θ is not zero on CS frame at no-polarization. Because the correlation of electron-positron pair in the same signal-Hijing event is not completely subtracted from same signal-Hijing event. It is show that this subtraction method is needed to be more optimized, however, this effect from the correlation similarly influences all the polarization frames for each polarization case. Thus the relativistic λ_θ value to the values on the other frame for each other polarization case is useful. Therefore the CS frame is that the discrimination ability to observe the polarization is high.

It can also be referred to from $\lambda_{\theta\phi}$ and λ_ϕ. On GJ frame, $\lambda_{\theta\phi}$ is clearly non-zero. On the other hand, on HX frame and on CS frame, $\lambda_{\theta\phi}$ is zero within uncertainties at all the

polarization cases. $\lambda_{\theta\phi}$ shows the deviation from the good frame, therefore HX frame and CS frame are good frames.

In addition, on HX frame and on GJ frame, λ_ϕ is not zero, nevertheless the polarization from magnetic field effect does not have the division of phi direction. This value of λ_ϕ is considered to be from the momentum division of the leptons pair. By contrast, λ_ϕ on CS frame has nearly the same value at all the polarization cases because CS frame is insulated from the influence of momentum distribution of the leptons pair.

From the above, CS frame is the best frame to measure the virtual photon polarization from magnetic field effect.

5.2 Polarization measurement with detectors

Next, I discuss the appearance at relativistic heavy ion collision experiments. In this thesis, the discussed experiment is ALICE experiment and PHENIX experiment. I simulate the polarization measurement with the limited rapidity η and ϕ according to the detector of each experiment.

5.2.1 ALICE detector

I simulate the polarization value λ_θ on CS frame at ALICE detector at first. This simulation is limited the rapidity η from -0.9 to 0.9. Because ALICE experiment mainly uses TPC to measure the charged particles. This result is Table 4 and Figure 36. Also, λ_θ on HX frame and GJ frame is described as reference.

polarization case	polarization frame	λ_θ
no-polarization	HX frame	-0.41 ± 0.030
	GJ frame	-0.41 ± 0.031
	CS frame	0.99 ± 0.085
perpendicular	HX frame	-0.40 ± 0.040
	GJ frame	-0.39 ± 0.040
	CS frame	1.7 ± 0.13
parallel	HX frame	-0.75 ± 0.032
	GJ frame	-0.72 ± 0.032
	CS frame	1.2 ± 0.29

Table 4: List of λ_θ at ALICE

At parallel polarization on CS frame, λ_θ becomes nearly the case of no-polarization. When the polarized parent particle goes to the beam axis, the z axis on CS frame is x axis on the laboratory system and the direction of a magnetic field is on yz plane on the laboratory system. In this situation, $cos\theta$ is 0 on CS frame. Also, at the parallel polarization, the direction of decayed particles is the same as the direction of the magnetic field. Thus, By cutting the rapidity region around the z axis, the probability that $cos\theta$ is 0 and nearly 0 is smaller. Therefore, the λ_θ varies and reaches nearly the value at no-polarization case at ALICE acceptance by this effect.

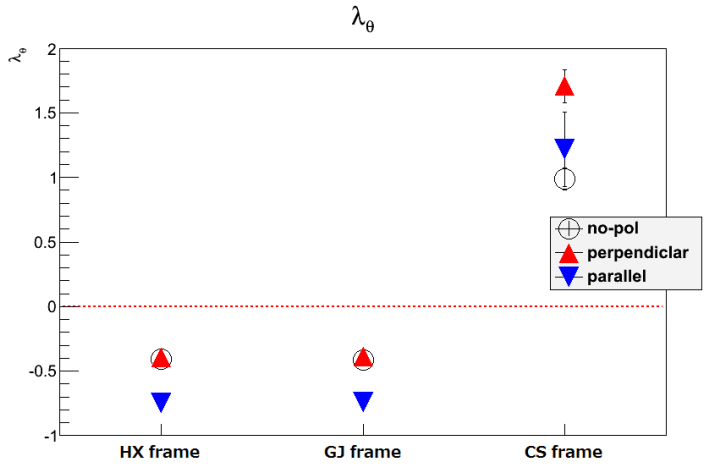

Figure 36: λ_θ at ALICE acceptance

5.2.2 PHENIX detector

I simulate the polarization value λ_θ at PHENIX detector next. This simulation is limited the rapidity $|\eta| < 0.375$ and $30° < |\phi| < 120°$. PHENIX experiment mainly uses DCH to measure the track of charged particles, and EMC and RHIC to identify the charged particles. Therefore the most smallest DCH acceptance in three detectors is applied. This result is Table 5 and Figure 37.

polarization case	polarization frame	λ_θ
no-polarization	HX frame	-0.43 ± 0.053
	GJ frame	-0.43 ± 0.056
	CS frame	1.2 ± 0.20
perpendicular	HX frame	-0.6 ± 0.10
	GJ frame	-0.6 ± 0.1
	CS frame	2.1 ± 0.26
parallel	HX frame	-0.93 ± 0.068
	GJ frame	-0.96 ± 0.070
	CS frame	-0.7 ± 0.47

Table 5: List of λ_θ at PHENIX acceptance

At PHENIX detector, λ_θ at parallel polarization on CS frame goes away from the others. The probability that $cos\theta$ is 0 and nearly 0 is smaller when the rapidity region is cut around the z axis. However, when the polarized parent particle goes to y axis on the laboratory system, the direction of the both beam axises and z axis on CS frame is on yz plane in the laboratory frame. Also, the direction of a magnetic field on xy plane is boosted by Lorentz transition and becomes nearly y axis on CS frame. In this situation, The $cos\theta$ is about 1.0. Therefore, $cos\theta$ exceeds 0.5, that is the reference point to measure polarization, at a certain point when the scattering direction of parents particle transports z axis to y axis. And the trend of λ_θ transition is reversed. This reverse is started when the rapidity is about 0.8. The PHENIX acceptance is the rapidity $|\eta| < 0.375$, this reversed

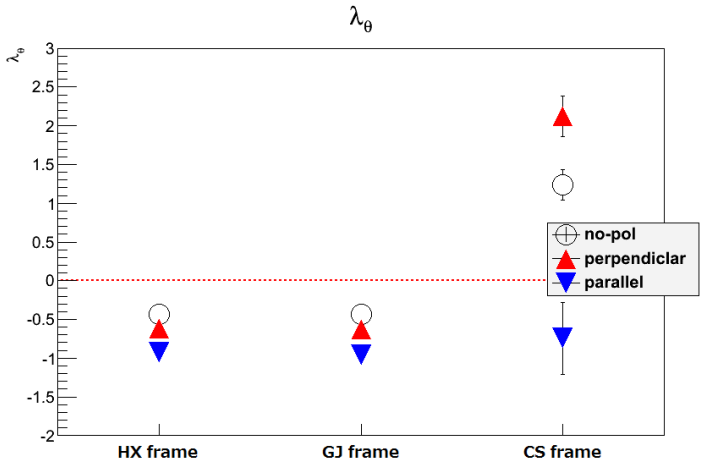

Figure 37: λ_θ at PHENIX

point is exceeded. Thus λ_θ at the parallel polarization on CS frame leaved from the value at the no-polarization.

5.3 With polarization rate

In this section, I discuss the polarization measurement in consideration of polarization rate of virtual photon. In the region that $0.12 < M_{e^+e^-} < 0.3\ GeV/c^2$ and $1.0 < p_T < 5.0\ GeV/c$, the direct virtual photon is about one in 20 event[9] and the polarization rate of direct virtual photon is assumed to be 10%. Therefore, the polarized virtual photon is about one in 200 event. I simulate the polarization measurement with this condition like above.

These results is Table 6 and Figure 38. The λ_θ is nearly the same and zero within the uncertainty at all acceptance. The devision at ALICE and PHENIX is considered to be the effect of acceptance cut. Thus it means that the polarization measurement is difficult.

polarization case	polarization frame	λ_θ at all acceptance	λ_θ at ALICE	λ_θ at PHENIX
no-polarization	HX frame	-0.1 ± 0.39	0.3 ± 0.73	0.2 ± 0.58
	GJ frame	-0.1 ± 0.44	0.3 ± 0.65	0.3 ± 0.43
	CS frame	0.2 ± 0.25	-0.08 ± 0.83	-0.4 ± 0.51
perpendicular	HX frame	-0.09 ± 0.41	0.6 ± 0.94	0.2 ± 0.65
	GJ frame	-0.06 ± 0.45	0.5 ± 0.74	0.3 ± 0.56
	CS frame	0.2 ± 0.27	-0.3 ± 0.98	-0.3 ± 0.50
parallel	HX frame	-0.2 ± 0.41	0.2 ± 0.98	0.03 ± 0.48
	GJ frame	-0.2 ± 0.46	0.2 ± 0.65	0.1 ± 0.43
	CS frame	0.08 ± 0.27	-0.4 ± 0.66	-0.5 ± 0.46

Table 6: List of λ_θ at with acceptance cut

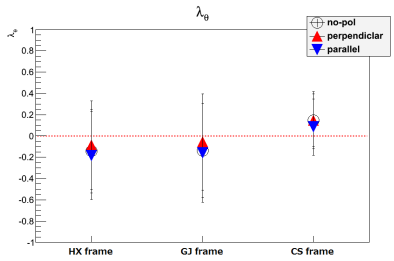

λ_θ at all acceptance

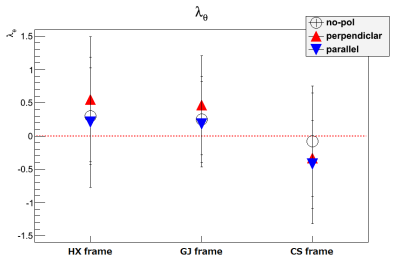

λ_θ at ALICE acceptance

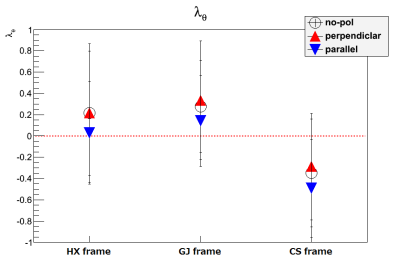

λ_θ at PHENIX acceptance

Figure 38: λ_θ at all, ALICE and PHENIX acceptance

6 Conclusion

In this thesis, the theoretical feasibility of polarization measurement is discussed and the best frame to observe polarization is found. Also, the polarization measurement is simulated with the polarization rate, one polarized pair in 200 event. From these results, the theoretical feasibility is enough large, 0.6σ using the data in 2010 and more using the data in 2014, and CS frame is the best frame to do it. On the other hand, the simulation with the polarization rate shows that the polarization measurement is difficult because the polarization rate is low. However, it does not mean that polarization frames are meaningless to measure the virtual photon polarization. In this thesis the method for direct virtual photon selection is p_T and mass cut only. Therefor the possibility of polarization measurement exists when more effective selection is used and the polarization rate becomes high.

To measure the polarization, it needs to develop use the better method of direct virtual photon selection. Also it is important that the statistics are increased, and the subtraction method of the correlation of signal pair is optimizes. When these succeed, the polarization measurement will succeed to use the polarization frame.

7 Acknowledgement

I would like to thank associate Prof. K.Shigaki. He purposed to me the theme of this thesis, and he gave me many advises. I could not have done this thesis without his support. Also, I would like to appreciate Prof. T.Sugitate. He taught me the method of presentation and advised for this thesis. These are important and valuable. Assistant Prof. K.Homma discussed with me about the physics for this thesis, and gave me suggestions. And I am grateful to Assistant Prof. T.Miyoshi for his comments at the meeting. I would like to express my gratitude.

And I would like to appreciate whom I worked together in the Hiroshima group. Hoshino-san and Nagashima-san taught me about the detectors and physics. Matsuura-san discussed with me the thesis, physics and anything. I had enjoyed working with her. Yamakawa-kun and Nobuhiro-kun also discussed with me anything. Especially, Yamakawa-kun gave me suggestions for this thesis.

I am grateful to other people. I can not appreciate all of them enough. Thank you everyone, again.

References

[1] Japan group of LHC ALICE experiment "http://alice-j.org"

[2] Y.Yamaguchi, Tokyo University, doctor thesis(2011),
"Direct photon measurement with virtual photon method in d+Au collisions at $\sqrt{s_{NN}} = 200GeV$ "

[3] RHIC STAR experiment "http://www.star.bnl.gov"

[4] 'MAGNETARS', SOFT GAMMA REPEATERS & VERY STRONG MAGNETIC FIELDS
"http://solomon.as.utexas.edu/magnetar.html"

[5] http://lambda.phys.tohoku.ac.jp/kaneta/pukiwiki/index.php?FrontPage

[6] Tsuji, Asako, the master's thesis (2014),
"Evaluations and mesurements of virtual photon polarization dou to intense magnetic field in Pb+Pb collisions at $\sqrt{s_{NN}} = 2.76TeV$ with ALICE"

[7] A. Adare et al. (PHENIX Collaboration) Phys. Rev. Lett. 104, 132301 (2010)

[8] N. M. Kroll and W. Wada, Phys.Rev., vol. 98, pp. 1355-1359, 1955

[9] A. Adare et al. (PHENIX Collaboration) Phys. Rev. C 81, 034911 (2010)

[10] Afanasiev, S. et al. (PHENIX Collaboration) Phys.Rev. C80, 024909 (2009)

[11] http://qd.typepad.com/5/2005/12/the_fight_for_r.html

[12] KEK group of RHIC PHENIX experiment
"https://www.kek.jp/ja/Facility/IPNS/RHIC-PHENIX/"

[13] L. Aphecetche et al. (PHENIX Collaboration), Nucl.Instrum.Meth. A499 (2003) 521-536
"PHENIX calorimeter"

[14] M. Aizawa et al. (PHENIX Collaboration), Nucl.Instrum.Meth. A499 (2003) 508-520
"PHENIX central arm particle ID detectors"

[15] K. Adcox et al. (PHENIX Collaboration), Nucl.Instrum.Meth. A499 (2003) 489-507
"HENIX central arm tracking detectors"

[16] K. Aamodt (Oslo U.)et al. (ALICE Collaboration), JINST 3 (2008) S08002
"The ALICE experiment at the CERN LHC"

[17] P. Faccioli, C. Lourenạo, J. Seixas and H.K. Währi, Eur. Phys. J. C 69, 657(2010)

[18] P. Faccioli et al., Int. Workshop on Heavy Quarkonia 2008
"J/Ψ polarization measurements revisited"